Clinical Radiology 74 (2019) 651.e7–651.e14

Contents lists available at ScienceDirect

Clinical Radiology

journal homepage: www.clinicalradiologyonline.net

Glioma grading and *IDH1* mutational status: assessment by intravoxel incoherent motion MRI

X. Wang, X.-Z. Chen, L. Shi, J.-P. Dai*

Department of Neuroimaging, Beijing Tiantan Hospital, Capital Medical University, Beijing 100050, China

ARTICLE INFORMATION

Article history:
Received 27 November 2018
Accepted 22 March 2019

AIM: To assess the diagnostic performance of intravoxel incoherent motion (IVIM) magnetic resonance imaging (MRI) in differentiating high-grade gliomas (HGGs) from low-grade gliomas (LGGs), and predicting the isocitrate dehydrogenase 1 (*IDH1*) mutational status.

MATERIALS AND METHODS: IVIM imaging was performed preoperatively in 42 patients with gliomas using 10 b-values (0–1,200 s/mm^2) in a 3 T MRI machine. The perfusion fraction (f), true diffusion coefficient (D), pseudo-diffusion coefficient (D*), and apparent diffusion coefficient (ADC) were calculated within the tumours and in the contralateral normal white matter, and the values were compared between the HGGs and LGGs, and between IDH1 wild-type and mutated-type gliomas. In addition, the receiver operating characteristic (ROC) was also analysed.

RESULTS: When compared to LGGs, HGGs had lower ADC (0.989×10^{-3} versus 1.243×10^{-3} mm^2/s, $p<0.001$), smaller D (0.849×10^{-3} versus 1.062×10^{-3} mm^2/s, $p=0.001$), larger D* (9.731×10^{-3} versus 5.442×10^{-3} mm^2/s, $p=0.006$), and bigger f-values (0.204 versus 0.130, $p<0.001$) within the tumours. The area under the receiver operating characteristic (ROC) curve (AUC) was 0.937, 0.898, 0.770, and 0.838, respectively. Among the LGGs, tumours with the *IDH1* mutation had a higher ADC (1.286×10^{-3} mm^2/s), when compared to the wild-type *IDH1* (1.122×10^{-3} mm^2/s, $p=0.003$), with an AUC of 0.936. In HGGs, tumours with the *IDH1* mutation had higher ADC (1.056×1010^{-3} versus 0.946×10^{-3} mm^2/s, $p=0.030$), smaller D* (6.204×10^{-3} versus 11.999×10^{-3} mm^2/s, $p=0.023$) and smaller f-values (0.143 versus 0.244, $p<0.001$), with an AUC of 0.766, 0.841 and 0.992, respectively.

CONCLUSION: Glioma grading can be differentiated and *IDH1* mutational status can be predicted using IVIM.

Introduction

Gliomas are the most common primary neoplasms of the brain, which histologically vary from low grade to high grade, according to the World Health Organization (WHO) classification.[1] Recent studies have focused on the genetic basis of tumorigenesis in gliomas, as it contributes to the histological classification of gliomas.[2] The 2016 Central Nervous System (CNS) WHO classification of gliomas is

* Guarantor and correspondent: J.-P. Dai, Department of Neuroimaging, Beijing Tiantan Hospital, Capital Medical University, No. 6 Tiantan Xili, Chongwen District, Beijing, 100050, China. Tel.: +86 010 67098843; fax: +86 010 67098843.

E-mail address: neuro_d2004@163.com (J.-P. Dai).

https://doi.org/10.1016/j.crad.2019.03.020
0009-9260/

based on both histological and molecular features, particularly the isocitrate dehydrogenase 1 (*IDH1*) mutation status,[3] both of which are clinically important for tumour treatment and patient prognosis.[4–6] Radiologically, gliomas can be graded by diffusion-weighted imaging (DWI), diffusion kurtosis imaging (DKI), and dynamic susceptibility contrast (DSC) magnetic resonance imaging (MRI)[7–9]; however, these techniques cannot obtain perfusion and dispersion parameters through a sequence.

Le Bihan *et al.*[10] proposed intravoxel incoherent motion (IVIM) to describe the microscopic translational motion, which included molecular diffusion of water and microcirculation of blood in the capillary network. Based on the bi-exponential model, the IVIM technique can extract three parameters D, D*, and f. D was called the diffusion coefficient, which is related to molecular diffusion restriction, D* was called the pseudodiffusion coefficient, which was related to the movement of blood in the microvasculature, and f was called the perfusion fraction, which described the fraction of incoherent signal that arises from the vascular compartment in each voxel over the total incoherent signal. Studies have demonstrated that f correlated well with DSC CBV; f and D*correlated well with dynamic contrast-enhanced MRI-derived Ktrans in glioma.[11,12]

IVIM permits the acquisition of perfusion and diffusion information in a time-efficient manner, and in a single sequence.[10] Furthermore, IVIM perfusion does not require contrast media, which is valuable for patients with a contraindication to gadolinium-chelate contrast medium injection. To date, this technique has been used to grade gliomas, but the results remain inconsistent.[13–15] To the authors' knowledge, no study has used IVIM MRI to predict the mutational status of *IDH1* at present. Hence, the present study aimed to grade the gliomas and predict the *IDH1* mutational status using IVIM.

Materials and methods

Patients

The present study was approved by the institutional review board, and informed consent was obtained from each participant. This study was conducted in accordance with the declaration of Helsinki.

Between December 2016 and January 2018, patients with suspected primary supratentorial gliomas, who underwent brain MRI examinations, were included into the present study. Patients were excluded when they had a previous history of relevant biopsies or therapies, or had contraindications to MRI (claustrophobia, metal implants, or pacemakers). Among the 76 consecutive patients initially recruited for the present study, 28 patients were excluded due to histopathological diagnosis other than gliomas according to the WHO criteria or no neurosurgical resection, and six patients were excluded due to head movement artefacts. A total of 42 patients (age: 46.4±12.1 years old; 22 males and 20 females) with histopathologically confirmed glioma were enrolled. Among these 42 patients, 19 patients (age: 43±11.1 years old; 10 males and nine females) had low-grade glioma (LGG; Grade II) and 23 patients (age: 49.3±12.4 years old; 12 males and 11 females) had high-grade glioma (HGG; Grade III and IV). In addition, among these 23 patients, nine patients with HGG (age: 46.2±14.2 years old; four males and five females) had mutated *IDH1* mutations, whereas the remaining 14 patients (age: 51.2±11.2 years old; eight males and six females) had the wild-type gene. In contrast, among the 19 patients, 14 patients with LGG (age: 43.9±11.1 years old; eight males and six females) had mutated *IDH1*, while the remaining five patients (age: 40.4±11.89 years old; two males and three females) had wild-type *IDH1*. The histological types of gliomas of these patients were as follows: 11 diffuse astrocytomas, four oligodendrogliomas, four oligoastrocytoma, six anaplastic astrocytoma, four anaplastic oligoastrocytomas, and 13 glioblastoma multiforme (GBM).

MRI parameters

All MRI data were acquired using a 3 T MRI machine (Discovery MR750 System, GE Medical Systems) with a 32-channel head coil. The protocol consisted of an IVIM scan, followed by a conventional scan. The IVIM imaging was performed in axial planes through a single-shot echo-planar imaging diffusion sequence, with 10 b-values (0, 20, 50, 100, 150, 200, 500, 800, 1,000, and 1,200 s/mm^2) in three orthogonal directions. With the increase in b-values, the number of excitations (NEX) also increased from one to three. The repetition time (TR) and echo time (TE) were 2,500 ms and 59 ms, respectively.

The conventional MRI protocol was as follows: axial T1-weighted imaging (TR=1,750 ms, TE=19.6 ms), axial T2-weighted imaging (TR=7,900 ms, TE=140 ms), axial T2 fluid-attenuated inversion recovery imaging (TR/TE=8,000/145 ms, inversion time [TI]=2,000 ms), and three orthogonal plane contrast-enhanced gradient-echo T1-weighted imaging (TR/TE=1,777/19.6 ms). The section thickness (5 mm), intersection gap (1.5 mm) and field of view (FOV; 240×240 mm) were uniform in all sequences of the conventional scanning protocol.

Data processing

All imaging data were processed and analysed using the workstation (Advantage Workstation 4.6, GE Medical

Table 1
IVIM-derived parameters in low- and high-grade gliomas.

	Parameters	LGGs	HGGs	*p*-Value
Within tumours	ADC ($\times10^{-3}$ mm^2/s)	1.243±0.116	0.989±0.121	<0.001
	D ($\times10^{-3}$ mm^2/s)	1.062±0.243	0.849±0.125	0.001
	D* ($\times10^{-3}$ mm^2/s)	5.442±2.115	9.731±6.143	0.006
	F	0.130±0.037	0.204±0.072	<0.001
Normal white matter	ADC ($\times10^{-3}$ mm^2/s)	0.767±0.059	0.759±0.030	0.611
	D ($\times10^{-3}$ mm^2/s)	0.667±0.057	0.653±0.041	0.346
	D* ($\times10^{-3}$ mm^2/s)	5.210±1.664	4.927±1.375	0.550
	F	0.124±0.019	0.117±0.012	0.144

IVIM, intravoxel incoherent motion; HGG, high-grade glioma; LGG, low-grade glioma; f, perfusion fraction; D, true diffusion coefficient; D*, pseudo-diffusion coefficient; ADC, apparent diffusion coefficient.

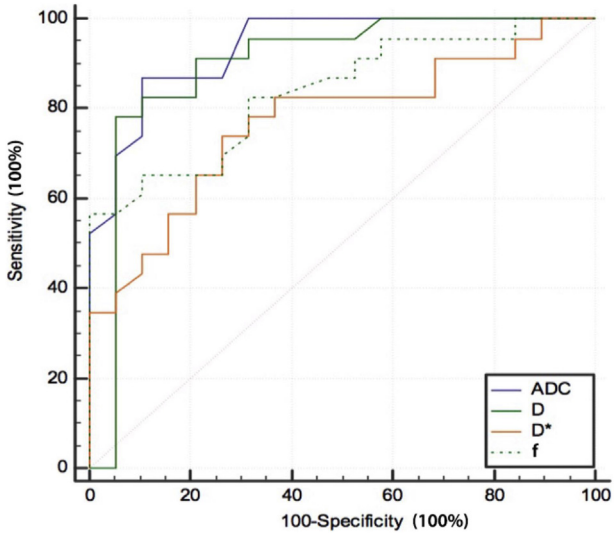

Figure 1 ROC analysis for distinguishing HGGs from LGGs.

Table 2
ROC analysis for distinguishing HGGs from LGGs.

	AUC (95%CI)	Sensitivity (%)	Specificity (%)	Cut-off value
ADC	0.937 (0.817–0.989)	86.96	89.47	1.090
D	0.898 (0.765–0.970)	78.26	94.74	0.935
D*	0.770 (0.614–0.886)	73.91	73.68	6.160
F	0.838 (0.691–0.933)	56.52	100.0	0.189

ROC, receiver operating characteristic; AUC, area under the ROC curve; HGG, high-grade glioma; LGG, low-grade glioma; f, perfusion fraction; D, true diffusion coefficient; D*, pseudo-diffusion coefficient; ADC, apparent diffusion coefficient.

Systems) by two radiologists (with 5 and 11 years of experience in neurological MRI image interpretation, respectively) in consensus. Similar to previous studies,[14,16,17] five freehand (regions of interest) ROIs (30–40 mm^2) were carefully placed on the solid parts of the tumours. The solid portion was defined as the enhancing region of the tumour on contrast-enhanced T1-weighted images. For non-enhancing tumours, the ROI was drawn at the centre of the portion where the T2 or T2-fluid attenuated inversion recovery (FLAIR) signal abnormality was noted after careful inspection of the T1-, T2-and T2-FLAIR-weighted images.[12] The ROI was placed to cover as much of the solid part of the tumours as possible while avoiding areas of calcification, necrosis, cyst formation, haemorrhage and large vessels. The IVIM analysis used the MADC program implemented bi-exponential model to obtain the parametric maps. The maximum f and D*, and minimum ADC and D from all ROIs for each patient were recorded. The ADC, D, D* and f were also measured in a larger circular ROI (60 mm^2) placed in the contralateral normal white matter.

Histological characterisation

Surgically resected tumour tissues were processed and stained with haematoxylin and eosin (H&E), characterised as per standard protocols, and classified and graded according to the 2007 WHO criteria for central nervous system tumours.[18]

DNA pyro-sequencing for IDH1 mutation

Genomic DNA was isolated from frozen tumour tissues using the QIAamp DNA Mini Kit (Qiagen). The genomic region spanning the R132 mutation of *IDH1* was first amplified by PCR using the following primers: 5′-GCTTGTGAGTGGATGGGTAAAAC-3′ and 3′-biotin-TTGCCAACATGACTTACTTGATC-5′. The 40 μl PCR mixes comprised 1 μl of each 10 μM forward and reverse primers, 4 μl of 10×buffer, 3.2 μl of 2.5 mM dNTPs, 2.5 U of hotstart Taq (Takara), and 2 μl of 10 μM template DNA. The PCR conditions were as follows: 95°C for 3 minutes; 50 cycles of 95°C for 15 seconds, 56°C for 20 seconds, 72°C for 30 seconds, and 72°C for 5 minutes (ABI PCR system 9700). Then, the biotinylated strand of the amplified DNA was purified from the total PCR product, and subjected to

Table 3
IVIM-derived parameters between wild-type and mutated-type *IDH1*.

			Mutated-type *IDH1*	Wild-type *IDH1*	*p*-Value
Within tumours	LGGs	ADC ($\times10^{-3}$ mm^2/s)	1.286±0.096	1.122±0.073	0.003
		D ($\times10^{-3}$ mm^2/s)	1.084±0.281	1.002±0.054	0.531
		D* ($\times10^{-3}$ mm^2/s)	4.852±1.788	7.094±2.259	0.093
		F	0.128±0.035	0.133±0.047	0.803
	HGGs	ADC ($\times10^{-3}$ mm^2/s)	1.056±0.103	0.946±0.115	0.030
		D ($\times10^{-3}$ mm^2/s)	0.892±0.130	0.822±0.119	0.199
		D* ($\times10^{-3}$ mm^2/s)	6.204±2.121	11.999±6.851	0.023
		F	0.143±0.029	0.244±0.064	<0.001
Normal white matter	LGGs	ADC ($\times10^{-3}$ mm^2/s)	0.764±0.058	0.775±0.065	0.734
		D ($\times10^{-3}$ mm^2/s)	0.662±0.051	0.683±0.075	0.483
		D* ($\times10^{-3}$ mm^2/s)	5.158±1.601	5.356±2.025	0.827
		F	0.122±0.015	0.130±0.027	0.452
	HGGs	ADC ($\times10^{-3}$ mm^2/s)	0.752±0.032	0.764±0.028	0.357
		D ($\times10^{-3}$ mm^2/s)	0.652±0.025	0.653±0.050	0.947
		D* ($\times10^{-3}$ mm^2/s)	5.324±2.123	4.672±0.497	0.277
		F	0.121±0.013	0.115±0.010	0.215

AUC, area under the receiver operating characteristic curve; IVIM, intravoxel incoherent motion; HGG, high-grade glioma; LGG, low-grade glioma; *IDH1*, isocitrate dehydrogenase 1 gene; f, perfusion fraction; D, true diffusion coefficient; D*, pseudo-diffusion coefficient; ADC, apparent diffusion coefficient.

pyrosequencing on the PyroMark Q24 ID System (QIAGEN) using the 5′-TGGATGGGTAAAACCT-3′ primer.

Statistical analysis

The ADC, D, D*, and f values of the intact white matter and tumours were compared for LGGs and HGGs by unpaired *t*-test, similar to that for tumours with different *IDH1* mutation statuses. $p<0.05$ was considered statistically significant. The receiver operating characteristic (ROC) analysis was performed to evaluate the diagnostic accuracy of the significantly different parameters using Medcalc (version 15.2.2; Ostend, Belgium). Area under the curve (AUC) values of <0.7, 0.7–0.9, and >0.9 were considered to indicate low, medium, and high diagnostic performance, respectively. Other data analyses were performed using the SPSS software (version 22; Chicago, IL, USA).

Results

The IVIM parameters (ADC, D, D*, and f) of the tumour lesions differed (Table 1) between LGGs and HGGs, but there was no significant difference in the contralateral normal white matter (Table 1). The ROC curves of the grading performances of ADC, D, D*, and f are presented in Fig 1 and Table 2. The ADC values revealed the highest diagnostic performance. The IVIM parameters (ADC, D, D*, and f) of tumour lesions with LGGs and HGGs and different *IDH1* statuses are presented in Table 3. The ADC values of both LGGs and HGGs were higher for mutated

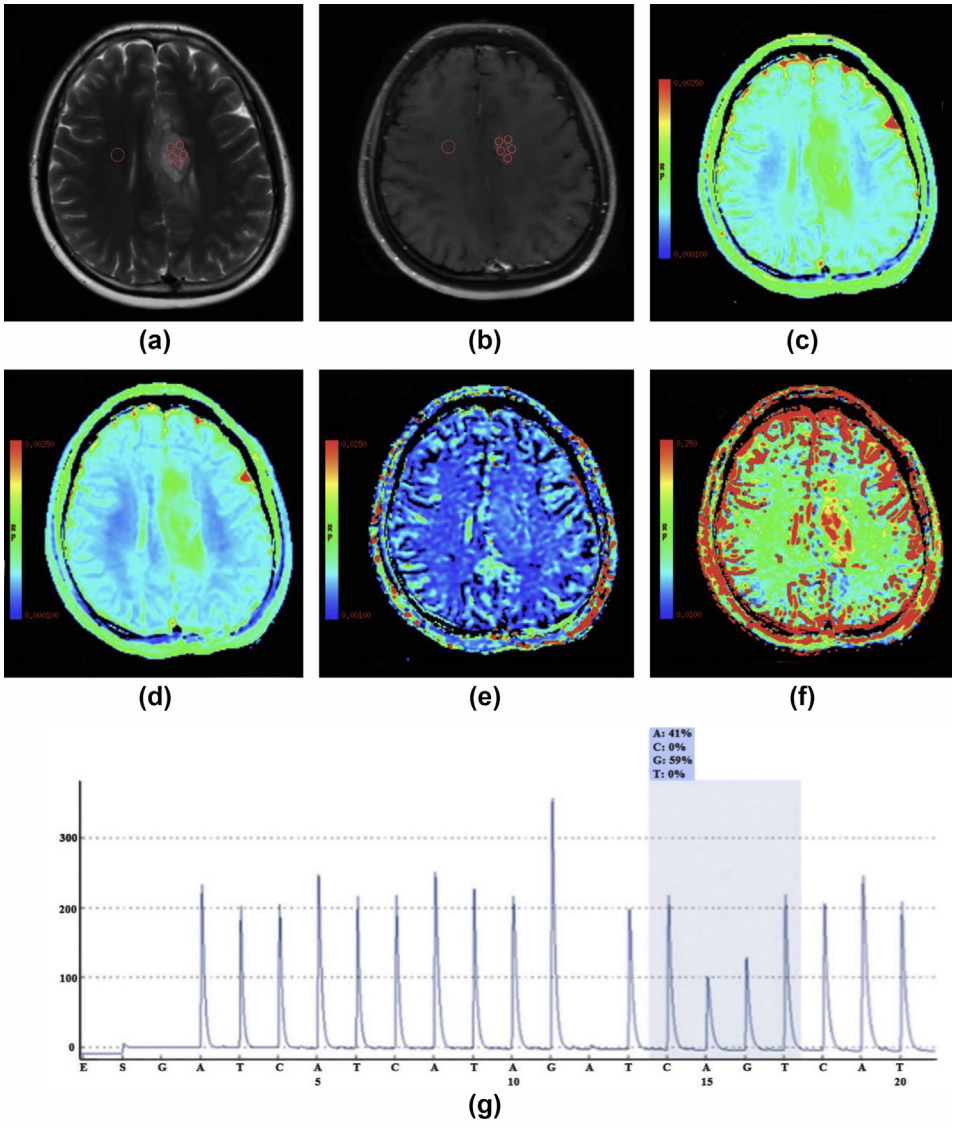

Figure 2 A case of HGG with *IDH1* mutation. (a) Axial T2WI. (b) Axial enhanced T1WI. (c) Axial ADC map. (d) The D map. (e) The D* map. (f) The f map. The maximum f and D*, and minimum ADC and D, from all ROIs were recorded. The ADC, D, D* and f values of the tumour were 1.090 ($\times10^{-3}$ mm^2/s), 0.869 ($\times10^{-3}$ mm^2/s), 4.660 ($\times10^{-3}$ mm^2/s) and 0.186 respectively. The ADC, D, D*, and f values of the contralateral normal white matter were 0.737 ($\times10^{-3}$ mm^2/s), 0.657 ($\times10^{-3}$ mm^2/s), 3.310 ($\times10^{-3}$ mm^2/s) and 0.117 respectively. (g) DNA pyro-sequencing indicated mutated *IDH1*.

IDH1, when compared to *IDH1* wild-type tumours. In contrast, the D* and f values were higher in wild-type *IDH1*, when compared to *IDH1* mutated tumours, in the HGG group (Figs 2 and 3). The parameters of normal-appearing white matter were not affected by the *IDH1* mutation status (Table 3).

The ROC curves for the diagnostic performance of each parameter in the LGG and HGG groups are presented in Figs 4 and 5, respectively, and the AUC, sensitivity, specificity, and suggested cut-off values for these parameters are presented in Table 4. Furthermore, ADC exhibited the highest accuracy in differentiating between *IDH1* mutated and *IDH1* wild-type tumours in LGGs (AUC: 0.936), and the f-value had best diagnostic performance in the HGG group (AUC: 0.992).

Discussion

Differentiating between HGGs and LGGs has important clinical implications in both the treatment and prognosis of gliomas. Previous studies have shown higher rCBF, higher rCBV, and lower ADC values in HGGs, when compared to LGGs[7,19,20]; however, the perfusion and diffusion parameters used in these studies were not simultaneously obtained by one MRI scanning sequence. In the present study, the IVIM MRI allowed for the simultaneous acquisition of diffusion and perfusion parameters, thereby providing both measurements within the corresponding solid lesions.

The present study revealed that the minimum ADC and D values were lower in HGGs, when compared to LGGs, while the maximum D* and f values were significantly higher in

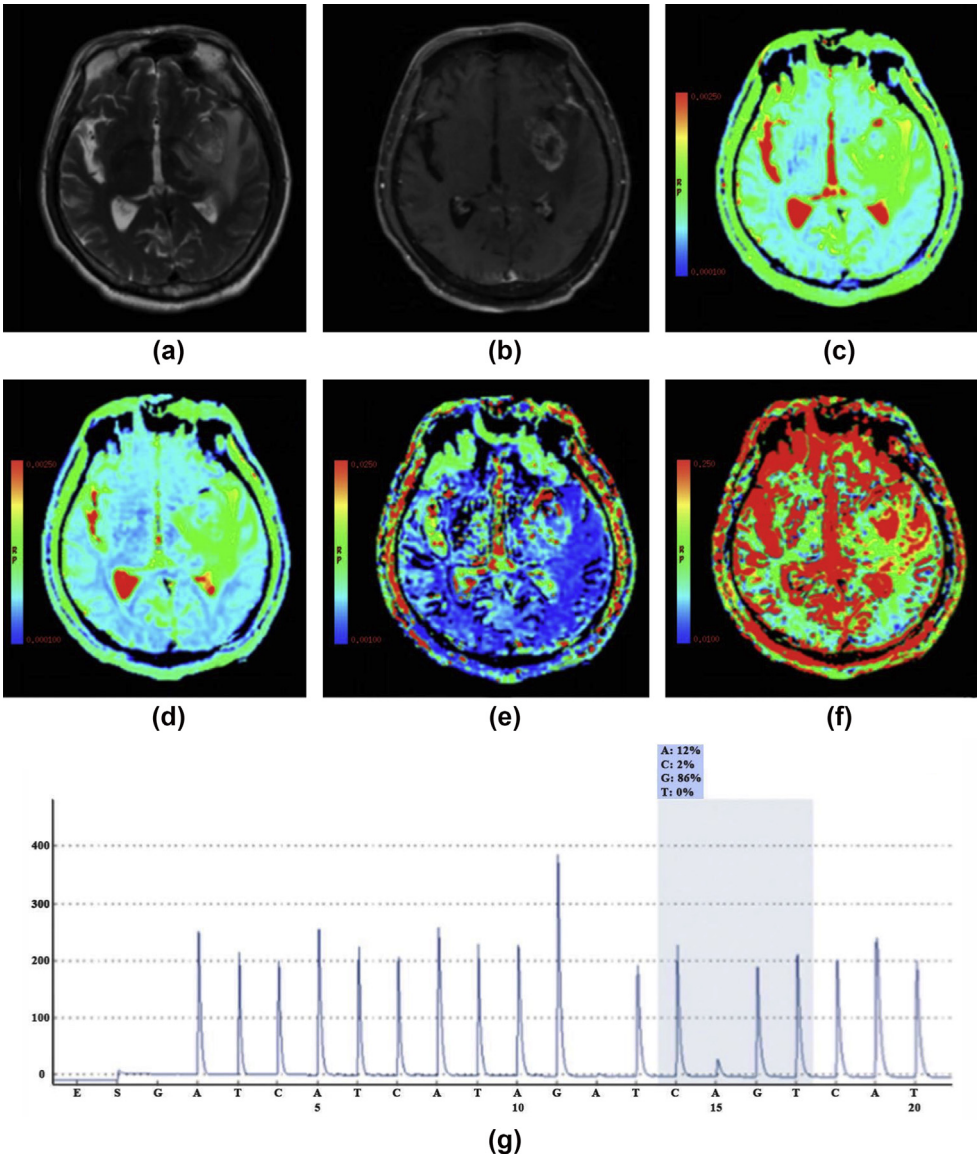

Figure 3 A case of HGG with wild-type *IDH1*. (a) Axial T2WI. (b) Axial enhanced T1WI. (c) Axial ADC map. (d) The D map. (e) The D* map. (f) The f map. The ADC, D, D*, and f values of the tumour were 0.828×10^{-3} (mm^2/s), 0.669 ($\times10^{-3}$ mm^2/s), 10.300 ($\times10^{-3}$ mm^2/s) and 0.350, respectively. The ADC, D, D*, and f values of the contralateral normal white matter were 0.725 ($\times10^{-3}$ mm^2/s), 0.541 ($\times10^{-3}$ mm^2/s), 4.950 ($\times10^{-3}$ mm^2/s) and 0.106 respectively. (g) DNA pyro-sequencing indicated wild-type *IDH1*.

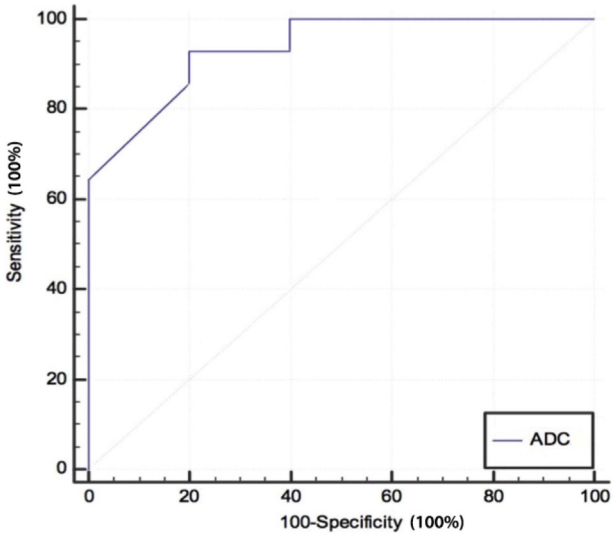

Figure 4 ROC analysis for distinguishing mutated *IDH1* from wild-type *IDH1* in the LGGs. The ADC value shows the best diagnostic performance with AUC 0.936.

the former. These findings were consistent with some previous studies,[14,15,17] but not with others.[13,21] The minimum ADC value was useful in identifying tumour areas with the highest cell attenuation or highest proliferation.[22] The lower ADC and D value in HGGs were likely due to higher cell density and volume, which constricts the intercellular spaces, and thereby impedes water movement. Several studies[13,14,22] have shown that D is smaller and more precise than ADC, which was mainly because ADC was estimated by a mono-exponential model with two b-values (usually 0 and 1,000 s/mm^2), and this estimation misrepresented both the diffusion and perfusion; however, in the present study, the ADC exhibited higher diagnostic

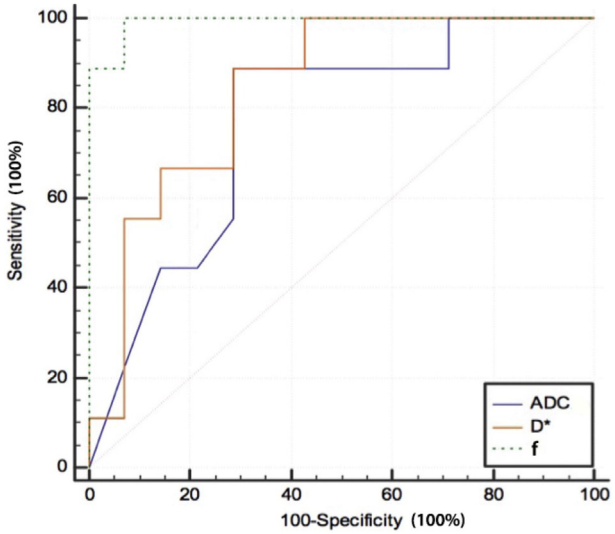

Figure 5 ROC analysis for distinguishing mutated *IDH1* from wild-type *IDH1* in the HGGs. The f value shows the highest diagnostic performance, with AUC 0.992. The ADC and D* values show moderate diagnostic performance, with AUCs 0.766 and 0.841, respectively.

Table 4
ROC analysis for distinguishing mutated *IDH1* from wild-type *IDH1*.

		AUC (95%CI)	Sensitivity (%)	Specificity (%)	Cut-off value
LGGs	ADC	0.936 (0.723–0.997)	92.86	80	1.180
HGGs	ADC	0.766 (0.545–0.915)	88.89	71.43	0.955
	D*	0.841 (0.630–0.959)	88.89	71.43	8.140
	f	0.992 (0.837–1.000)	100	92.86	0.186

ROC, receiver operating characteristic; AUC, area under the ROC curve; HGG, high-grade glioma; LGG, low-grade glioma; *IDH1*, isocitrate dehydrogenase 1 gene; f, perfusion fraction; D, true diffusion coefficient; D*, pseudo-diffusion coefficient; ADC, apparent diffusion coefficient.

performance, when compared to the D value. Nevertheless, the sentiment that D can be used instead of ADC remain worthy of further study.

Furthermore, D* was significantly higher in HGGs, when compared to LGGs, which is consistent with the effect of intra-tumour microvessel density (MVD) on D* values[15]; however, some studies have indicated that D* is unstable due to its high sensitivity to capillary blood flow, as well as the partial volume effects of CSF and necrosis, which make it more SNR demanding than the f value.[13,14] Therefore, it is necessary to develop a reliable method to quantify D* in tumours. As the f value refers to the volume fraction of the rapid diffusion component in voxel, it could also reflect the perfusion in tumour tissues. Several studies have shown a positive correlation between f and CBV, and significantly higher values in the HGGs,[14,15,23,24] indicating that it might be a reliable quantitative parameter to evaluate the vascularity of gliomas.

Significant radiological differences were also found between *IDH1* mutated and wild-type tumours in both HGGs and LGGs. Mutations in *IDH1* can induce a neomorphic enzyme activity that converts α-ketoglutarate (α-KG) to (R)-2-hydroxyglutarate ((R)-2HG), which is known to target pro-angiogenic hypoxia-inducible factor 1-alpha (HIF-1A).[25] Zhao *et al.*[26] revealed that *IDH1* mutations led to a partial decrease in angiogenesis via the induction of the HIF-1 pathway. In GBM patients, the *IDH1* mutation is associated with a lower proliferation rate, when compared to wild-type tumours.[27] A study suggested that *IDH1* gene mutations may reflect alterations in metabolism, cellularity, and angiogenesis, and that tumours with *IDH1* mutation are composed of a more heterogeneous microenvironment.[28] Therefore, *IDH1* mutated gliomas exhibited a higher ADC, when compared to wild-type tumours, regardless of the glioma grade. Furthermore, in both LGGs and HGGs, the D values of tumours with *IDH1* mutations were higher than those with wild-type *IDH1*, although statistical significance was not reached due to the small sample size.

It was also found that the D* and f values of *IDH1* mutated tumours were lower, when compared to wild-type *IDH1*, only in HGGs, while the f value exhibited the best diagnostic performance among all parameters. This finding was consistent with previous studies that reported significantly lower rCBV values in gliomas with *IDH1* mutation relative to gliomas with *IDH1* wild-type[29–31]; however, contrary to the findings of Tan *et al.*,[32] it was found that the perfusion parameters were not affected by the *IDH1*

mutation status in LGGs. This could be due to the fact that the microvascular proliferation in LGGs is less prominent, when compared to HGGs. Moreover, the LGGs recruited in the present study were all grade II gliomas, which included astrocytoma, oligodendroglioma, and oligoastrocytoma, contrary to previous studies.[29,30]

The present results demonstrate that both the diffusion and perfusion parameters of IVIM imaging are useful for differentiating HGGs from LGGs, and predicting the *IDH1* mutation status. It is noteworthy that the quantitative ability of IVIM imaging could be affected by imaging parameters, especially for the selection and number of b-values. Suo *et al.*[33] revealed in their studies that a b-value of 200 s/mm^2 may be considered as an appropriate point to separate perfusion decay and diffusion decay in signal attenuation curves with a wide range of b-values. In the present study, 10 b-values were used, including six that ranged from 0 to 200 s/mm^2 and four that ranged from 500 to 1,200 s/mm^2; however, the optimal number of b-values for IVIM remains undetermined, and further research is warranted to clarify this issue.

The present study had a few limitations. First, the sample was small. Therefore, a larger cohort should be studied to validate these present findings. Second, previous research reported that oligodendroglioma and oligoastrocytoma had higher levels of metabolic activity and angiogenesis than astrocytoma.[32] In this study, both LGGs and HGGs consisted of different histological types, resulting in significant heterogeneity that may have influenced the results. Finally, other clinically relevant mutations (e.g., vascular endothelial growth factor and epidermal growth factor receptor) and epigenetic alterations (such as the methylation of the oxygen-6-methylguanine–DNA methyl transferase promoter) associated with gliomas were not taken into consideration, despite the possible influence on imaging parameters.

In conclusion, IVIM imaging can be used as a non-invasive quantitative imaging method for differentiating HGGs from LGGs, and predicting the *IDH1* mutation status by simultaneously providing diffusion and perfusion parameters.

Conflict of interest

The authors declare no conflict of interest.

Acknowledgements

This research was supported by High Level Health Technical Personnel Training Funding of Beijing Municipal Health Department of China (2015-3-042 [X.C.]). This research was also supported by National Natural Science Foundation of China (81772005).

References

1. Daumas-Duport C, Scheithauer B, O'Fallon J, *et al.* Grading of astrocytomas. A simple and reproducible method. *Cancer* 1988;**62**(10):2152–65 [PubMed:3179928].
2. Louis DN. The next step in brain tumour classification: "Let us now praise famous men"... or molecules? *Acta Neuropathol* 2012;**124**(6):761–2. https://doi.org/10.1007/s00401-012-1067-4 [PubMed:23151844].
3. Louis DN, Perry A, Reifenberger G, *et al.* The 2016 World Health organization classification of tumours of the central nervous system: a summary. *Acta Neuropathol* 2016;**131**(6):803–20. https://doi.org/10.1007/s00401-016-1545-1 [PubMed:27157931].
4. Oike T, Suzuki Y, Sugawara K, *et al.* Radiotherapy plus concomitant adjuvant temozolomide for glioblastoma: Japanese mono-institutional results. *PLoS One* 2013;**8**(11):e78943, https://doi.org/10.1371/journal.pone.0078943 [PubMed:24265731].
5. Nageswara Rao AA, Packer RJ. Advances in the management of low-grade gliomas. *Curr Oncol Rep* 2014;**16**(8):398. https://doi.org/10.1007/s11912-014-0398-9 [PubMed:24925153].
6. Karsy M, Guan J, Cohen AL, *et al.* New molecular considerations for glioma: IDH, ATRX, BRAF, TERT, H3 K27M. *Curr Neurol Neurosci Rep* 2017;**17**(2):19. https://doi.org/10.1007/s11910-017-0722-5 [PubMed:28271343].
7. Zhang L, Min Z, Tang M, *et al.* The utility of diffusion MRI with quantitative ADC measurements for differentiating high-grade from low-grade cerebral gliomas: evidence from a meta-analysis. *J Neurol Sci* 2017;**373**:9–15. https://doi.org/10.1016/j.jns.2016.12.008 [PubMed:28131237].
8. Bai Y, Lin Y, Tian J, *et al.* Grading of gliomas by using monoexponential, biexponential, and stretched exponential diffusion-weighted MR imaging and diffusion kurtosis MR imaging. *Radiology* 2016;**278**(2):496–504. https://doi.org/10.1148/radiol.2015142173 [PubMed:26230975].
9. Friedman SN, Bambrough PJ, Kotsarini C, *et al.* Semi-automated and automated glioma grading using dynamic susceptibility-weighted contrast-enhanced perfusion MRI relative cerebral blood volume measurements. *Br J Radiol* 2012;**85**(1020):1204–11. https://doi.org/10.1259/bjr/13908936 [PubMed:23175486].
10. Le Bihan D, Breton E, Lallemand D, *et al.* MR imaging of intravoxel incoherent motions: application to diffusion and perfusion in neurologic disorders. *Radiology* 1986;**161**(2):401–7. https://doi.org/10.1148/radiology.161.2.3763909 [PubMed:3763909].
11. Federau C, O'Brien K, Meuli R, *et al.* Measuring brain perfusion with intravoxel incoherent motion (IVIM): initial clinical experience. *J Magn Reson Imaging* 2014;**39**(3):624–32. https://doi.org/10.1002/jmri.24195 [PubMed:24068649].
12. Cao M, Suo S, Han X, *et al.* Application of a simplified method for estimating perfusion derived from diffusion-weighted MR imaging in glioma grading. *Front Aging Neurosci* 2017;**9**:432. https://doi.org/10.3389/fnagi.2017.00432 [PubMed:29358915].
13. Bisdas S, Koh TS, Roder C, *et al.* Intravoxel incoherent motion diffusion-weighted MR imaging of gliomas: feasibility of the method and initial results. *Neuroradiology* 2013;**55**(10):1189–96. https://doi.org/10.1007/s00234-013-1229-7 [PubMed:23852430].
14. Togao O, Hiwatashi A, Yamashita K, *et al.* Differentiation of high-grade and low-grade diffuse gliomas by intravoxel incoherent motion MR imaging. *Neuro Oncol* 2016;**18**(1):132–41. https://doi.org/10.1093/neuonc/nov147 [PubMed:26243792].
15. Federau C, Meuli R, O'Brien K, *et al.* Perfusion measurement in brain gliomas with intravoxel incoherent motion MRI. *AJNR Am J Neuroradiol* 2014;**35**(2):256–62. https://doi.org/10.3174/ajnr.A3686 [PubMed:23928134].
16. Shen N, Zhao L, Jiang J, *et al.* Intravoxel incoherent motion diffusion-weighted imaging analysis of diffusion and microperfusion in grading gliomas and comparison with arterial spin labeling for evaluation of tumour perfusion. *J Magn Reson Imaging* 2016;**44**(3):620–32. https://doi.org/10.1002/jmri.25191 [PubMed:26880230].
17. Zou T, Yu H, Jiang C, *et al.* Differentiating the histologic grades of gliomas preoperatively using amide proton transfer-weighted (APTW) and intravoxel incoherent motion MRI. *NMR Biomed* 2018;**31**(1):e3850, https://doi.org/10.1002/nbm.3850 [PubMed:29098732].
18. Louis DN, Ohgaki H, Wiestler OD, *et al.* The 2007 WHO classification of tumours of the central nervous system. *Acta Neuropathol* 2007;**114**(2):97–109. https://doi.org/10.1007/s00401-007-0243-4 [PubMed:17618441].

19. Kong L, Chen H, Yang Y, *et al*. A meta-analysis of arterial spin labelling perfusion values for the prediction of glioma grade. *Clin Radiol* 2017;**72**(3):255–61. https://doi.org/10.1016/j.crad.2016.10.016 [PubMed:27932251].
20. Santarosa C, Castellano A, Conte GM, *et al*. Dynamic contrast-enhanced and dynamic susceptibility contrast perfusion MR imaging for glioma grading: preliminary comparison of vessel compartment and permeability parameters using hotspot and histogram analysis. *Eur J Radiol* 2016;**85**(6):1147–56. https://doi.org/10.1016/j.ejrad.2016.03.020 [PubMed:27161065].
21. Lin Y, Li J, Zhang Z, *et al*. Comparison of intravoxel incoherent motion diffusion-weighted MR imaging and arterial spin labeling MR imaging in gliomas. *Biomed Res Int* 2015;**2015**:1–10. https://doi.org/10.1155/2015/234245 [PubMed:25945328].
22. Hu YC, Yan LF, Wu L, *et al*. Intravoxel incoherent motion diffusion-weighted MR imaging of gliomas: efficacy in preoperative grading. *Sci Rep* 2014;**4**:7208. https://doi.org/10.1038/srep07208 [PubMed:25434593].
23. Puig J, Sanchez-Gonzalez J, Blasco G, *et al*. Intravoxel incoherent motion metrics as potential biomarkers for survival in glioblastoma. *PLoS One* 2016;**11**(7):e0158887, https://doi.org/10.1371/journal.pone.0158887 [PubMed:27387822].
24. Wu WC, Yang SC, Chen YF, *et al*. Simultaneous assessment of cerebral blood volume and diffusion heterogeneity using hybrid IVIM and DK MR imaging: initial experience with brain tumours. *Eur Radiol* 2017;**27**(1):306–14. https://doi.org/10.1007/s00330-016-4272-z [PubMed:26905869].
25. Rohwer N, Zasada C, Kempa S, *et al*. The growing complexity of HIF-1alpha's role in tumorigenesis: DNA repair and beyond. *Oncogene* 2013;**32**(31):3569–76. https://doi.org/10.1038/onc.2012.510 [PubMed:23160373].
26. Zhao S, Lin Y, Xu W, *et al*. Glioma-derived mutations in IDH1 dominantly inhibit IDH1 catalytic activity and induce HIF-1alpha. *Science* 2009;**324**(5924):261–5. https://doi.org/10.1126/science.1170944 [PubMed:19359588].
27. Yan W, Zhang W, You G, *et al*. Correlation of IDH1 mutation with clinicopathologic factors and prognosis in primary glioblastoma: a report of 118 patients from China. *PLoS One* 2012;**7**(1):e30339, https://doi.org/10.1371/journal.pone.0030339 [PubMed:22291938].
28. Lee S, Choi SH, Ryoo I, *et al*. Evaluation of the microenvironmental heterogeneity in high-grade gliomas with IDH1/2 gene mutation using histogram analysis of diffusion-weighted imaging and dynamic-susceptibility contrast perfusion imaging. *J Neurooncol* 2015;**121**(1):141–50. https://doi.org/10.1007/s11060-014-1614-z [PubMed:25205290].
29. Xing Z, Yang X, She D, *et al*. Noninvasive assessment of IDH mutational status in World Health Organization Grade II and III astrocytomas using DWI and DSC-PWI combined with conventional MR imaging. *AJNR Am J Neuroradiol* 2017;**38**(6):1138–44. https://doi.org/10.3174/ajnr.A5171 [PubMed:28450436].
30. Kickingereder P, Sahm F, Radbruch A, *et al*. IDH mutation status is associated with a distinct hypoxia/angiogenesis transcriptome signature which is non-invasively predictable with rCBV imaging in human glioma. *Sci Rep* 2015;**5**:16238. https://doi.org/10.1038/srep16238 [PubMed:26538165].
31. Yamashita K, Hiwatashi A, Togao O, *et al*. MR Imaging-based analysis of glioblastoma multiforme: estimation of IDH1 mutation status. *AJNR Am J Neuroradiol* 2016;**37**(1):58–65. https://doi.org/10.3174/ajnr.A4491 [PubMed:26405082].
32. Tan W, Xiong J, Huang W, *et al*. Noninvasively detecting Isocitrate dehydrogenase 1 gene status in astrocytoma by dynamic susceptibility contrast MRI. *J Magn Reson Imaging* 2017;**45**(2):492–9. https://doi.org/10.1002/jmri.25358 [PubMed:27367599].
33. Suo S, Cao M, Zhu W, *et al*. Stroke assessment with intravoxel incoherent motion diffusion-weighted MRI. *NMR Biomed* 2016;**29**(3):320–8. https://doi.org/10.1002/nbm.3467 [PubMed:26748572].